

## Coercivity exceeding 100 kOe in epitaxially grown FePt sputtered films

T. Shima<sup>a)</sup> and K. Takanashi

*Institute for Materials Research, Tohoku University, Sendai 980-8577, Japan*

Y. K. Takahashi and K. Hono

*National Institute for Materials Science, 1-2-1 Sengen, Tsukuba 305-0047, Japan*

(Received 5 January 2004; accepted 29 July 2004)

Microstructure and magnetization processes of highly ordered FePt (001) films with large perpendicular magnetic anisotropy have been studied. The film morphology was controlled from assemblies of single-domain nanoparticles to those of multidomain islands by varying the nominal thickness ( $t_N$ ) of the FePt films sputter-deposited on a heated MgO (001) substrate. The change in the magnetization process from magnetization rotation to domain wall displacement is clearly demonstrated by the initial magnetization curves. Huge coercivities as high as 70 and 105 kOe have been achieved in the film with single-domain particles at room temperature and 4.5 K, respectively. © 2004 American Institute of Physics. [DOI: 10.1063/1.1794863]

The magnetization process of assemblies of ferromagnetic nanoparticles with a large uniaxial magnetocrystalline anisotropy is of great scientific and technological interest, since they are expected to be applied in forthcoming magnetic devices such as high density magnetic recording media and high performance biasing nano-magnets. It is well known that the magnetization process and the coercivity depend strongly on the characteristic size and the morphology of the assemblies of ferromagnetic particles. Recently, a lot of investigations have been made to process FePt films and particles by conventional thin film preparation techniques<sup>1-6</sup> and a chemical synthesis technique,<sup>7</sup> since the L1<sub>0</sub> ordered FePt phase possesses a large uniaxial magnetocrystalline anisotropy. However, only a few investigations have realized high coercivity<sup>8-10</sup> together with highly aligned crystal orientation. In our previous work,<sup>9</sup> we reported that high coercivity ( $H_c$ ) exceeding 40 kOe was achieved in highly ordered FePt (001) films with the island structure that were epitaxially grown on MgO (001) substrates. However,  $H_c$  was still only one-third of the value expected from the coherent rotation model<sup>2</sup> ( $2K_u/M_s \sim 120$  kOe;  $K_u$ : uniaxial magnetic anisotropy,  $M_s$ : saturation magnetization). The present study focuses on a further improvement in coercivity by approaching the ideal morphology with the coherent rotation of single-domain particles. High magnetic field measurements were performed to evaluate the huge coercivity obtained from isolated single domain particles, and the magnetization processes are discussed based on the initial magnetization curves.

FePt films were prepared by co-sputtering Fe and Pt targets directly onto single crystalline MgO (001) substrates using a high vacuum (base pressure  $\sim 5 \times 10^{-10}$  Torr) multiple dc-sputtering system. High-purity argon of 1.4 m Torr was flown during sputtering. The substrates were heated to 780 °C during the deposition. The nominal thickness of FePt film ( $t_N$ ) was varied in the range between 1 and 40 nm. The compositions of the films were determined to be Fe<sub>52</sub>Pt<sub>48</sub> (at. %) by electron probe x-ray microanalysis (EPMA). The typical growth rate for FePt was 0.12 nm/s. The structural analy-

sis was performed by transmission electron microscopy (TEM) and x-ray diffraction with Cu-K $\alpha$  radiation. Magnetization curves were measured by a vibrating sample magnetometer (VSM) equipped with a superconducting magnet (maximum magnetic field of  $\pm 140$  kOe) at temperatures of 4.5 and 295 K.

In-plane TEM bright field images of the FePt films with different  $t_N$  deposited on a MgO (001) substrate are shown in Fig. 1.  $t_N$  is 1 nm (a), 3 nm (b), 5 nm (c), and 20 nm (d). Note that the scale of each micrograph is different. The films are grown with the island growth mode at  $T_s=780^\circ\text{C}$  as reported in our previous work for  $T_s=700^\circ\text{C}$ .<sup>9</sup> The particle size of the film with  $t_N=1$  nm is smaller than 5 nm. With increasing  $t_N$ , the typical size of particles increases from 10 to 20 nm for  $t_N=3$  nm to 20 to 30 nm for  $t_N=5$  nm. Strongly faceted islands of FePt particles with large size distribution are observed for  $t_N=3$  and 5 nm. With further increase of  $t_N$ , a number of small particles coalesced to form big particles. The distribution of the particles with  $t_N=20$  nm is bimodal, consisting of larger ones with a typical size of about 200 nm

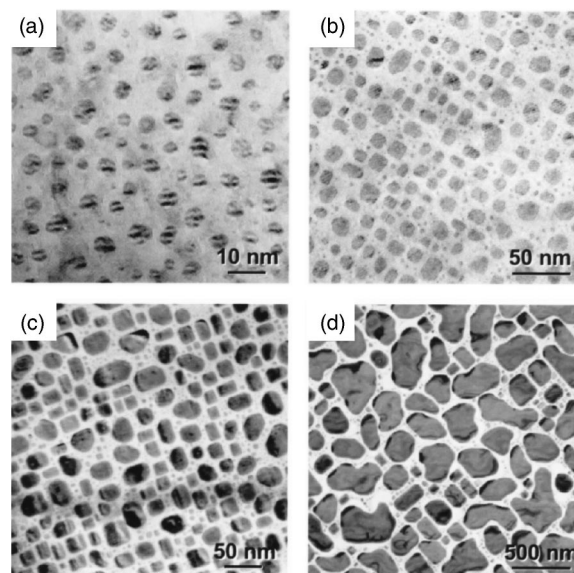


FIG. 1. In-plane TEM bright field images for the FePt films with different thickness:  $t_N=1$  nm (a), 3 nm (b), 5 nm (c), and 20 nm (d).

<sup>a)</sup> Author to whom correspondence should be addressed; electronic mail: shima@imr.tohoku.ac.jp

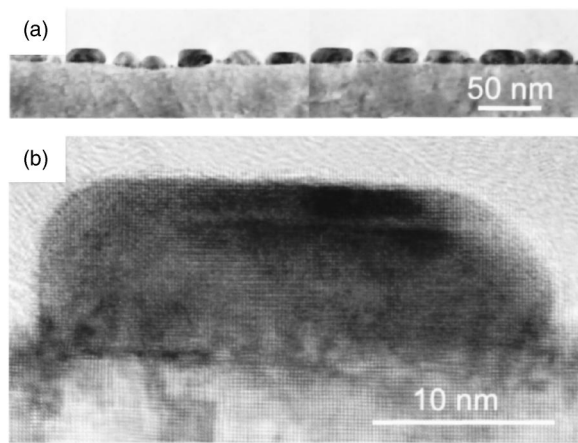


FIG. 2. Cross-sectional TEM images of the FePt film with  $t_N=5$  nm.

in side and smaller ones with a  $\{001\}$  faceted morphology whose size ranges from 10 to 50 nm. In comparison with the microstructure of the films deposited at  $T_s=700^\circ\text{C}$ ,<sup>9</sup> there is little strain contrast in the particles grown at  $780^\circ\text{C}$ .

Cross-sectional TEM images of the film with  $t_N=5$  nm are shown in Figs. 2(a) and 2(b). Although the sizes of particles are scattered as shown in Fig. 1, the heights of large particles are almost the same ( $\sim 15$  nm). The enlarged cross-sectional image [Fig. 2(b)] clearly shows the contrast corresponding to the alternating atomic stacking of Fe and Pt layers in the  $[001]$  direction of the  $L1_0$  structure. Furthermore, no structural defects, such as twins, are observed and the surfaces of the particles are atomically flat. From the integrated intensities of the fundamental and superlattice peaks extracted from the numerical fitting of x-ray diffraction patterns (the figure not shown), the degree of long-range chemical order  $S$  was estimated to be  $0.95\pm 0.05$  for all the samples.

Figure 3 shows magnetization curves for the films with  $t_N=1$  nm (a), 3 nm (b), 5 nm (c), 20 nm (d), and 40 nm (e) measured at 295 K. The solid and broken lines are the magnetization curves with magnetic fields applied in the perpendicular and parallel directions to the film plane, respectively. The magnetic easy axes are perpendicular to the film plane for all the samples. Among the curves, the film with  $t_N=1$  nm [Fig. 3(a)] shows a different nature: low saturation magnetization of less than 500 emu/cc and low  $H_c$  of 18 kOe. TEM observation revealed that the sizes of the particles for  $t_N=1$  nm were mostly smaller than 5 nm in diameter. The different behavior of the magnetization curve is thought to arise from the insufficient  $L1_0$  ordering, in other words the existence of small particles with poor chemical order. It was recently reported that FePt particles smaller than  $\sim 4$  nm were not ordered to the  $L1_0$  structure.<sup>11</sup> A huge  $H_c$  of 64 kOe was observed for the film with  $t_N=3$  nm [Fig. 3(b)] in the perpendicular direction. The particle size of this film was smaller than 20 nm. The step of the perpendicular magnetization curve around zero magnetic field is thought to arise from the mixture of fully  $L1_0$  ordered particles and small particles with poor chemical ordering as described before. However, with increasing  $t_N$ , the step of the magnetization curve around zero magnetic field disappears and the maximum  $H_c$  of 70 kOe is achieved for the film with  $t_N=5$  nm [Fig. 3(c)]. With further increasing  $t_N$ , the  $H_c$  decreases slowly, but still keeps a quite large value of about

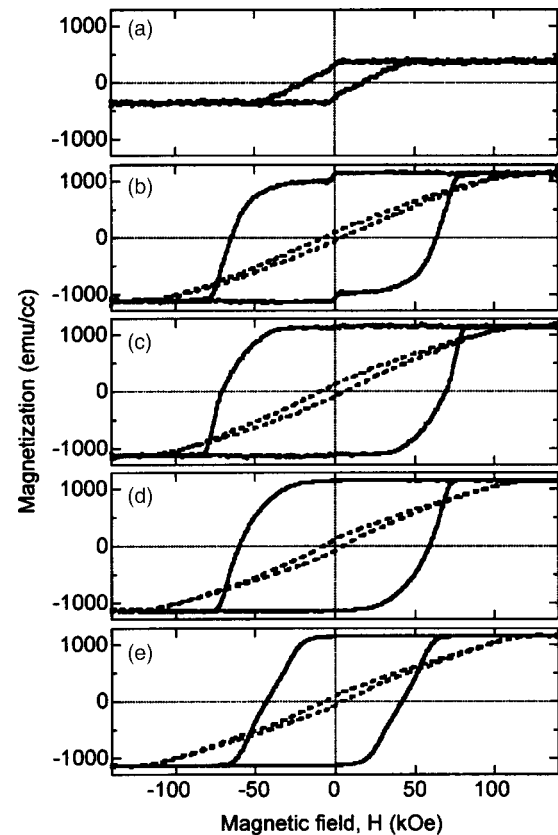


FIG. 3. Magnetization curves at 295 K for the FePt films with  $t_N=1$  nm (a), 3 nm (b), 5 nm (c), 20 nm (d), and 40 nm (e).

43 kOe for  $t_N=40$  nm [Fig. 3(e)]. The large  $H_c$  can be achieved until the percolation of the film morphology occurs between  $t_N=50$  and 70 nm. The saturation magnetization for the films with  $t_N\geq 3$  nm is about 1150 emu/cc and the maximum energy product  $(BH)_{\max}$  reaches about 50 MGOe, which is almost equal to the ideal value  $(2\pi M_s)^2$ . The saturation magnetic fields  $H_s$  measured in the in-plane direction (magnetic hard axis) for the films with  $t_N\geq 3$  nm are about 120 kOe. The uniaxial magnetic anisotropy  $K_u$  determined from the area enclosed between the magnetization curves in applied fields parallel and perpendicular to the film plane does not change with increasing  $t_N$ . The films for  $t_N\geq 3$  nm showed a large value of  $6.2\pm 0.2\times 10^7$  erg/cc, which is very close to the value of fully ordered FePt alloys ( $7.0\times 10^7$  erg/cc).

From the magnetic force microscopy (MFM) observation, it has been revealed that the multidomain particles are formed when the particle size becomes larger than approximately 200 nm.<sup>12</sup> The difference between the magnetization processes in single-domain particles and multidomain particles is demonstrated clearly by the initial magnetization curves shown in Fig. 4. All the magnetization curves were measured at 295 K in the perpendicular direction to the film plane. The vertical axis indicates the magnetization normalized by the magnetization value at the magnetic field of 140 kOe.  $t_N$  is 3 nm (a), 5 nm (b), 8 nm (c), 10 nm (d), 12 nm (e), 15 nm (f), 18 nm (g), 20 nm (h), 25 nm (i), 30 nm (j), and 40 nm (k). The films with  $t_N=3$  and 5 nm are very difficult to be magnetized [Fig. 4(a) and 4(b)], because they contain only single domain particles with the sizes of ten to a few tens of nanometers. Hence, the magnetization progresses only by the magnetization rotation in the par-

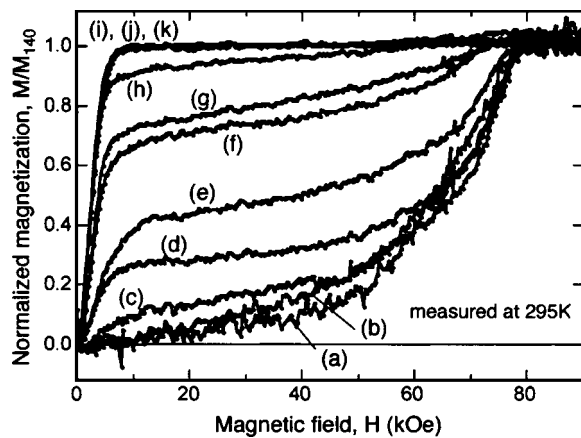


FIG. 4. Initial magnetization curves for the FePt films with  $t_N=3$  nm (a), 5 nm (b), 8 nm (c), 10 nm (d), 12 nm (e), 15 nm (f), 18 nm (g), 20 nm (h), 25 nm (i), 30 nm (j), and 40 nm (k).

ticles. However, with increasing  $t_N$  [(c) 8 nm and (d) 10 nm], i.e., with increasing particle size, a steep increase of the magnetization at low magnetic field is observed although the complete saturation is still hard. The fractional magnetization at low magnetic field corresponds to the magnetic domain wall displacement; in other words, particles larger than 200 nm with multidomain structure are magnetized at low magnetic field. With further increasing  $t_N$  [(f) 15 nm and (h) 20 nm], the volume fraction of multidomain particles increases and consequently, the fraction of the magnetization that is magnetized at low magnetic field increases. Figure 4(h) indicates that the small particles less than 200 nm with single-domain structure still exist for the film with  $t_N=20$  nm because there is a small fraction of the magnetization that is hard to saturate. This is consistent with the TEM observation as shown in Fig. 1(d). However, they disappear for the films with  $t_N \geq 25$  nm (i, j, k). In this case, the magnetization can be easily saturated at lower than 10 kOe with the displacement of domain walls. These initial magnetization curves are usually classified as “nucleation-type.” The observation of initial magnetization process gives significant information about the co-existence of both single-domain and multidomain structures, which cannot be distinguished from the MFM observation because of the present insufficient resolution. Furthermore, it is noted that the value of  $K_u$  keeps almost constant although the magnetic domain structure changes from single- to multidomain state, indicating that the magnetization process depends exclusively on the film morphology.

Although the largest  $H_c$  of 70 kOe was observed for  $t_N=5$  nm at room temperature [Fig. 3(c)], it was further enhanced by measuring at a cryogenic temperature. Figure 5 shows the magnetization curve for the film with  $t_N=5$  nm measured at 4.5 K. It was measured in the perpendicular direction to the film plane. With decreasing temperature,  $H_c$  increases remarkably and huge  $H_c$  of 105 kOe was achieved. This enhancement is thought to arise from the reduction of the thermal fluctuation, and also the increase in uniaxial magnetic anisotropy energy  $K_u$  with decreasing temperature. However, at this moment, it is hard to discuss the origin for the temperature dependence of  $H_c$ , because of the difficulty of precise determination of anisotropy field  $H_A$  at low temperature. Since the signal of the magnetization in the in-

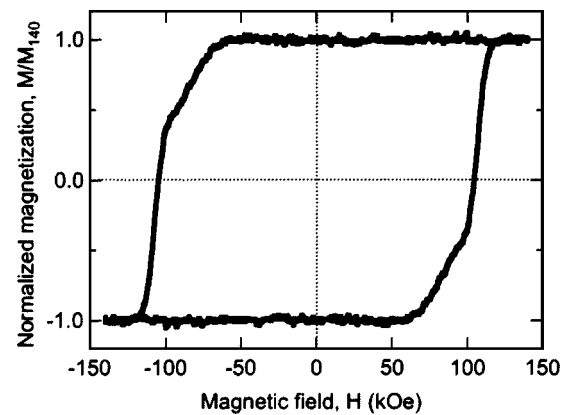


FIG. 5. Magnetization curves for the FePt film with  $t_N=5$  nm measured at 4.5 K.

plane direction was too small and the contribution of the magnetic impurities in the MgO substrate was enormous at low temperature, we were not able to measure  $H_A$  at low temperature. The value of  $H_c$  and  $H_A$  for  $t_N=5$  nm at room temperature is 70 and 120 kOe, respectively. The ratio of  $H_c/H_A$  is 0.58, which is considerably larger compared to the value obtained in commercial hard magnetic materials. This is because commercial magnets contain a lot of defects that can induce magnetic reversal. On the other hand, it is possible to produce nearly ideal ferromagnetic particle assemblies using the  $L1_0$  FePt phase.

This work has revealed that a huge coercivity exceeding 100 kOe can be obtained in defect-free perfectly aligned single domain particles. From the initial magnetization behavior, the change in the magnetization process from rotation of magnetization to domain wall displacement has been clearly demonstrated.

This work was partly supported by “Nanohetero Metallic Materials” from the MEXT. The structural characterization was performed at Laboratory for Advanced Materials, IMR, Tohoku University. High field magnetic measurement was performed at CLTS, Tohoku University. The authors would like to acknowledge Dr. S. Sugimoto for fruitful discussion; Y. Murakami for technical assistance.

<sup>1</sup>B. M. Lairson, M. R. Viosokay, R. Sinclair, and B. M. Clemens, Appl. Phys. Lett. **62**, 639 (1993).

<sup>2</sup>C. P. Luo and D. J. Sellmyer, IEEE Trans. Magn. **31**, 2764 (1995).

<sup>3</sup>J.-U. Thiele, L. Folks, M. F. Toney, and D. K. Weller, J. Appl. Phys. **84**, 5686 (1998).

<sup>4</sup>B. Bian, K. Sato, Y. Hirotsu, and A. Makino, Appl. Phys. Lett. **75**, 3686 (1999).

<sup>5</sup>T. Shima, T. Moriguchi, S. Mitani, and K. Takanashi, Appl. Phys. Lett. **80**, 288 (2002).

<sup>6</sup>T. Seki, T. Shima, K. Takanashi, Y. Takahashi, E. Matsubara, and K. Hono, Appl. Phys. Lett. **82**, 2461 (2003).

<sup>7</sup>S. Sun, C. B. Murray, D. Weller, L. Folks, and A. Moser, Science **287**, 1989 (2000).

<sup>8</sup>Y. Ide, T. Goto, K. Kikuchi, K. Watanabe, J. Onagawa, H. Yoshida, and J. M. Cadogan, J. Magn. Magn. Mater. **177-181**, 1245 (1998).

<sup>9</sup>T. Shima, K. Takanashi, Y. K. Takahashi, and K. Hono, Appl. Phys. Lett. **81**, 1050 (2002).

<sup>10</sup>S. Okamoto, O. Kitakami, N. Kikuchi, T. Miyazaki, Y. Shimada, and Y. K. Takahashi, Phys. Rev. B **67**, 094422 (2003).

<sup>11</sup>Y. K. Takahashi, T. Ohkubo, M. Ohnuma, and K. Hono, J. Appl. Phys. **93**, 7166 (2003).

<sup>12</sup>G. Q. Li, H. Takahashi, H. Ito, H. Saito, S. Ishio, T. Shima, and K. Takanashi, J. Appl. Phys. **94**, 5672 (2003).